PAPER

Quantitative modeling of neoclassical tearing mode driven fast ion transport in integrated TRANSP simulations

IOP Publishing Plasma Physics and Controlled Fusion
Plasma Phys. Control. Fusion **61** (2019) 055012 (13pp) https://doi.org/10.1088/1361-6587/ab0f08

Quantitative modeling of neoclassical tearing mode driven fast ion transport in integrated TRANSP simulations

L Bardóczi[1,2], M Podestà[3], W W Heidbrink[4] and M A Van Zeeland[1]

[1] General Atomics, PO Box 85608, San Diego, CA 92186-5608, United States of America
[2] Oak Ridge Associated Universities, Oak Ridge, TN 37831, United States of America
[3] Princeton Plasma Physics Lab, Princeton, NJ 08543, United States of America
[4] University of California, Irvine, CA 92697, United States of America

E-mail: bardoczil@fusion.gat.com

Received 30 November 2018, revised 21 February 2019
Accepted for publication 12 March 2019
Published 8 April 2019

Abstract

The TRANSP-'Kick' energetic particle transport model has been extended to study neoclassical tearing mode (NTM) driven fast ion (FI) transport with zero free parameters. FI transport induced by the NTM is obtained by calculating perturbed FI orbits via the guiding center particle following code ORBIT in the magnetic field of an experimentally characterized island chain. Transport probabilities are then used in TRANSP's Monte Carlo module NUBEAM to modify the FI distribution in every time step of the full TRANSP analysis. This procedure retains all TRANSP functionality and self-consistently predicts the NTM impact on beam torque, current drive and heating. Comparisons to DIII-D steady state, hybrid and ITER baseline plasmas are encouraging with the model quantitatively recovering the measured neutron rates. FI effects depend on the location and width of FI phase space resonances which are not accounted for by the former ad hoc beam diffusivity model of TRANSP. Resonance overlaps result in a transport threshold, for the cases investigated herein, at $W_{th} \approx 5$ cm. When $W < W_{th}$ the FI transport is dominated by energy and momentum redistribution. In particular, $m/n = 3/2$ NTMs lead to hollow T_{NB} profile at $q = m/n$ and broadened j_{NB} profile in the core. When $W > W_{th}$ FI losses increase, the neutral beam torque (T_{NB}) and driven current (j_{NB}) decrease across the entire plasma. The effects on NB profiles can strongly depend on the NTM frequency and mode numbers with the 3/2 (2/1) broadening (peaking) j_{NB} near the magnetic axis.

Keywords: magnetic island, ntm, fast ions, energetic particle, TRANSP, tokamak, transport

(Some figures may appear in colour only in the online journal)

1. Introduction

Magnetic islands driven by the neoclassical tearing mode (NTM) present a major concern for the operation of reactor-scale fusion devices as they can significantly decrease thermal [1–4] and energetic particles (EPs) [5–16] confinement and can lead to plasma termination [17]. NTM interaction with EPs impacts neutral beam (NB) torque (T_{NB}), heating and current drive (j_{NB}), which have important consequences on particle, thermal and momentum transport. The former ad hoc beam diffusivity (χ_{ab}) model of TRANSP [18, 19] simply broadens the NB profiles without sensitivity to NTM mode number, fast ion (FI) energy (E), canonical angular momentum (P_ζ) or magnetic moment (μ_B). The FI response to NTMs depends on details of the interaction, in particular on the location and width of wave-particle resonances in phase space, whose description requires a phase space resolved physics-based model. A rigorous calculation of these effects on FI slowing down timescales is challenging, particularly for experimental planning and analysis of many discharges, which motivates the development of reduced FI transport models.

The TRANSP-'Kick' reduced transport model [20, 21] was previously developed for Alfvén Eigenmode (AE) driven

FI transport, offering a path toward studying NTM–FI interaction and their effect on NB driven current, torque, heat and plasma equilibrium. In this paper we report the extension of the 'Kick'-model to include NTMs by integrating it with a new analysis tool of experimental island structure determination [22]. Magnetic islands are represented by a perturbed flux. For interpretive simulations, island evolution is an input and is prescribed entirely through measurements. For predictive simulations, one would have to adopt an NTM dynamic model to advance the island growth and rotation, as for example in recent TRANSP/MRE simulations [23]. E and P_ζ transfer probabilities between the FIs and the NTM are obtained by calculating perturbed FI orbits via the guiding center particle following code ORBIT in the perturbed magnetic field produced by the island chain. Interaction probabilities are then used in TRANSP's Monte Carlo module NUBEAM [24] to modify the FI distribution at every time step of the full TRANSP analysis. By taking integrals of the Monte Carlo FI distribution, the FI density, driven current, deposited energy, torque and other quantities are calculated. This model retains all TRANSP functionality and predicts the NTM impact on T_{NB}, j_{NB} and NB heating by self-consistently recomputing the sources and FI distribution, given measured thermal profiles and magnetic perturbation properties. This model was tested previously via phase space resolved diagnostics in repeat hybrid discharges [25]. In particular, the 'Kick'-model was in better agreement with red-shifted FIDA spatial profiles than the classical TRANSP data. Here, a series of tests were accomplished with a range of DIII-D plasma scenarios including ITER baseline (IBS), hybrid and ITER steady state with various NTMs (m/n= 2/1, 3/2 4/1 and 7/2) and realistic model NTM flux functions. The results are encouraging as the model quantitatively predicts the measured neutron rate ($\dot{N}$) without free parameters.

Below a threshold island width (W_{th}) the effect of the NTM is E and P_ζ redistribution, localized in the island region, without any radial redistribution or loss of particles. This threshold is at $W_{th} \approx 5$ cm for the examined IBS discharge heated with 80 keV deuterons. In the $W > W_{th}$ regime, FI transport is dominated by FI losses due to overlap of multiple phase space resonances, the effects of which are loss of j_{NB} and T_{NB} across a large portion of the plasma radius. The observed effects can strongly depend on mode frequency (f) and helicity. In particular, the 3/2 (2/1) leads to the broadening (peaking) of j_{NB} at the magnetic axis.

The paper is organized as follows. Analyzed DIII-D discharges are described in section 2 and the 'Kick'-model in section 3. We continue the paper with the test and validation of the 'Kick'-model in section 4. FI transport versus island width and rotation frequency are described in sections 4.1 and 4.2, respectively. Next, the 'Kick'-model is compared to the former ad hoc beam diffusivity model of TRANSP in section 4.3 and the impact of mode helicity is discussed in section 4.4. Finally, section 5 summarizes and concludes this paper. Numerical implementation of magnetic islands and experimental determination of their parameters are included in appendices A–C.

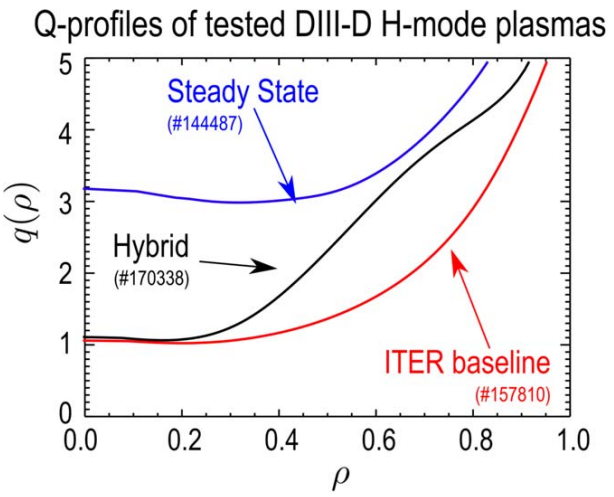

Figure 1. Q-profiles of different DIII-D H-mode scenario discharges with NTMs used to test the 'Kick'-model interpretive capability of NTM induced FI transport.

2. Experimental conditions

The TRANSP-'Kick' modeling capability is tested in a broad range of ITER relevant DIII-D H-mode plasmas: IBS, hybrid and steady state discharges. Example q-profiles of the analyzed discharges are shown in figure 1. The IBS has the highest performance with small central magnetic shear and low q_{95} (safety factor at $\rho = 0.95$). This type of discharge routinely develops $m/n = 2/1$ NTMs which can grow to a large size of $W \approx 10$ cm. Due to the low q_{95} and large W these modes are susceptible to locking to the wall which is often followed by plasma termination. The more stable steady state plasmas develop smaller islands, have higher q_{95}, lower plasma beta (β) and minimum safety factor (q_{min}) well above one. Hybrid discharges are in between the former two in terms of performance and stability. This pool of scenarios represent an excellent set of plasmas to test the 'Kick' FI transport model as wave-particle interaction in phase space depends sensitiviely on the q-profile.

Time traces of a highly reproducible, stationary hybrid plasma are shown in figure 2. The major radius coordinate of the magnetic axis was 179 cm, the plasma minor radius was $a = 58$ cm, elongation 1.85. In the stationary state the plasma current was $I_P = 1$ MA. $P_{beam} = 8$ MW NB power was injected and modulated with 10 Hz in the stationary part of the discharge (figure 2(a)). The chord averaged interferometry density was $n_e = 3.8 \times 10^{19}$ m^{-3} (interferometry [26]) (figure 2(b)), T_e (electron cyclotron emission, (ECE) [27]) and T_i (charge exchange recombination, CER [28]) at $q = 2$ were about 2.0 keV and 1.8 keV, respectively (figure 2(c)). The neutron rate ($\dot{N}$) is shown in figure 2(d). 80% of $\dot{N}$ comes from beam-target, 11% from beam-beam and 9% from thermonuclear fusion reactions.

Magnetic island structures form around $t = 1750$ ms at $q = 2$ with $n = 1$ toroidal mode number, which is consistent with a 2/1 NTM. The $n = 1$ signal measured at the tokamak wall via Mirnov-coils [29] is shown in figure 1(e). The full width of the saturated islands was $W \approx 11$ cm, as inferred

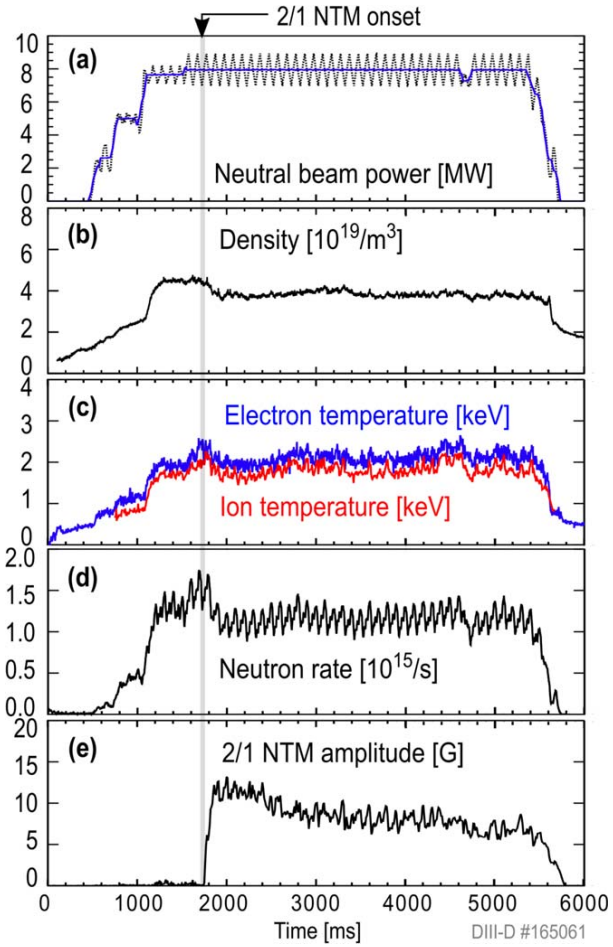

Figure 2. Time trace of (a) neutral beam power averaged over 50 ms (dotted) and 100 ms (solid), (b) density, (c) electron and ion temperature at $q = 2$, (d) neutron rate and (e) NTM amplitude in a hybrid plasmas.

from ECE and Mirnov measurements and modeling (appendix A). These islands were rotating with about 5 kHz (figure 3) and saturation occurred in about 100 ms at typically 12 G initially. After saturation, a quasi-stationary state of approximately 3 s followed, which provides adequate data for statistical analysis. The normalized square root of the toroidal (poloidal) flux surface label of the $q = 2$ rational surface was $\rho_s \approx 0.42$ ($\psi_s \approx 0.37$). ECE data indicates that this mode is the dominant helical MHD instability of the plasma. The $n = 2$ and $n = 3$ magnetic amplitudes are 10% and 0.7% of the $n = 1$ amplitude, respectively. The cross-power of line integrated interferometry density data in figure 3 shows nearly no coherent mode activity in the typical frequency range of AEs ($f \approx 50$–200 kHz), therefore any significant non-classical FI transport caused by AEs is ruled out and neglected in the analysis. Here, one interferometry channel looks horizontally in the tokamak mid-plane at the 225° toroidal port, while the other one looks vertically at the 240° toroidal port and is crossing the mid-plane at $R = 194$ cm major radius coordinate. Other interferometry signals and the ECE data are entirely free of AE activity. n_e, T_e, T_i and $\dot{N}$ all undergo a

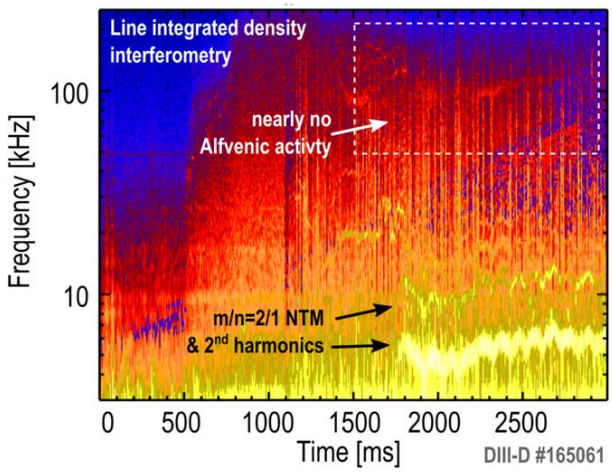

Figure 3. Cross-power of line integrated interferometry density signals shows that coherent density fluctuations are dominantly due to a ≈5 kHz mode. No significant activity is observed in the typical ($f \approx 50$–200 kHz) frequency range of Alfvén eigenmodes.

significant decrease when the NTM grows. These changes and comparison of $\dot{N}$ to the classical TRANSP analysis shows that the NTM has a significant impact on both the thermal and FI confinement, as will be shown in section 4. Therefore, these plasma conditions enable detailed tests of models for NTM induced FI transport. Setion 3 describes the TRANSP 'Kick' reduced FI transport model tested in this work.

3. TRANSP 'Kick'-reduced model of NTM driven FI transport

TRANSP [18, 19] is a time-dependent tokamak transport code used for particle, energy and momentum transport calculations. Inputs are the experimentally measured n_e, T_e, T_i, impurity density and rotation profiles, the magnetic equilibrium reconstruction, the beam injection geometry, current and voltage, and electron cyclotron heating power. The effect of MHD modes on the FI population is accounted for by the NUBEAM [24] module, where the FI distribution is evolved. This is accomplished in practice by modifying the FI distribution at every time step of the full TRANSP analysis as prescribed by a probability density matrix of E and P_ζ transfer rates between FIs and MHD modes. By taking integrals of the Monte Carlo FI distribution, the FI density, driven current, deposited energy, torque and other quantities are calculated.

The 'Kick'-model uses constants of motion of EPs to describe resonant wave-particle interaction in phase space. Each unperturbed orbit is characterized by 3 constants of motion: E, P_ζ and μ_B. The guiding center particle following code ORBIT [30] is used to calculate FI orbits in the perturbed magnetic field with random initial particle phases relative to the island. The magnetic reconstructions of the experimental MHD equilibrium is found using the code EFIT [31], constrained by internal measurements of the poloidal field radial profile by motional Stark effect spectroscopy [32] and by external magnetic probes [29]. Rotating magnetic

islands are implemented in this equilibrium through a perturbed flux Ψ, whose parameters are experimentally constrained (appendices A–C). ORBIT solves the Hamiltonian guiding center equations where the perpendicular electric field resulting from $d\mathbf{B}/dt$ is included. In this study the code is used in the ideal limit, where any parallel electric field perturbations ($\widetilde{E}_{\|}$) are canceled by the fast response of electrons along the magnetic field. $\widetilde{E}_{\|} = 0$ is set by introducing a Φ electrostatic potential [33] in the form:

$$\sum_{m,n} \alpha_{m,n} e^{i(n\phi - m\theta - \omega t)} - \mathbf{B} \cdot \nabla\Phi/\mathbf{B} = 0. \quad (1)$$

Here, $\xi = m\theta - n\phi$ is the island helical angle, θ (ϕ) is the poloidal (toroidal) angle. This is a simplification as NTMs are resistive magnetohydrodynamic instabilities. The equilibrium radial electric field (E_r) is also included which is calculated by TRANSP without islands based on CER data. These simulations neglect finite Larmor radius effects. These are expected to have no significant impact on the reported results as the strongest FI transport is driven by large islands where the finite Larmor radius effects are small, as confirmed by a set of test simulations. At fixed time intervals, the ΔE energy and ΔP_ζ momentum changes ('Kicks') are recorded and the probability density function of $p(E, P_\zeta, \mu_B|\Delta E, \Delta P_\zeta)$ is constructed in each bin in phase space at an arbitrarily chosen time (t_o) during the stationary state. The amplitude A of the E and P_ζ 'Kicks' is then rescaled in time proportionally with Ψ^2:

$$A(t) = A(t_o)(\Psi(t)/\Psi(t_o))^2 \quad (2)$$

$p(E, P_\zeta, \mu_B|\Delta E, \Delta P_\zeta, t)$ and $A(t)$ are used in the Monte Carlo module NUBEAM to modify the FI distribution in every time step of the full TRANSP analysis. The phase space structure of FI–NTM interaction is described in section 3.1.

3.1. Interaction of FIs with magnetic islands

Different classes of EPs including trapped, co-passing and counter-passing ions all strongly interact with the NTMs in all types of discharges. Resonances occur [33] where

$$\frac{\Delta\phi - \omega\Delta t/n}{\Delta\theta} = \frac{m'}{nl}. \quad (3)$$

$\Delta\phi$ and Δt are integrals on a closed orbit and l is any integer. These phase space wave-particle resonances give rise to a series of island chains in real space in the FI population with poloidal mode number m'. It is important to appreciate that the $m' \neq m$ resonant islands exist in the FI population only, not in T_e and not in $\widetilde{B}$ (perturbed magnetic field), therefore these can not be detected directly by ECE or Mirnov-coils. In contrast, thermal electrons follow the magnetic field lines, they can be used as tracers to map out the structure of $\widetilde{B}$. For example, a $2/1$ magnetic island is mapped out by thermal electrons in figure 4(a). This island is also seen in the passing ion orbits at all energy levels in the tested energy range. In addition to this $2/1$ magnetic island (which is implemented as a single harmonic $2/1$ magnetic perturbation), FI resonance leads to a secondary island chain in the FI orbits with $m/n = 3/1$ mode number at higher E, see the Poincarè map of 80 keV ($\mu B_o/E = 0.2$) co-passing ions in figure 4(b). This $3/1$ island is due to a resonance between the imposed $2/1$ island and counter-passing FIs as seen from the simultaneous emergence of a region of high energy transfer rate ($\dot{E}$) in the phase space of 80 keV ions at $P_\zeta < 0$ (not shown). Generally, every island chain in real space corresponds to a region in phase space where FIs strongly interact with the NTM (figure 4(c)).

The strength of resonances depends on E as shown by the energy transfer rate ($\dot{E}$) averaged in phase space over the co-passing, counter-passing and trapped particle domains (figure 5). $\dot{E}$ is very similar for co- and counter-passing FIs regardless of the width of the imposed island (figure 5(a)): $\dot{E}$ is nearly flat versus E with a small decrease (increase) at low (high) energies. In contrast, the interaction with trapped ions becomes weaker at higher E (figure 5(b)). Overall, the interaction is nearly constant versus E, implying that the results of section 4 are nearly independent from the NB injection energy.

The broader picture emerging from the 'Kick'-matrix is qualitatively similar to that of AEs [20] except that the interaction with NTMs is typically stronger due to the larger $\widetilde{B}$. The phase space resonances lead to perturbations in the NB heat, T_{NB}, and j_{NB} drive which have important consequences in thermal particle, energy and momentum transport calculations (section 4).

4. TRANSP 'Kick'-model validation and interpretive capabilities

TRANSP runs of IBS, hybrid and steady state plasmas in DIII-D with the 'Kick'-matrix are encouraging with the model quantitatively predicting the measured neutron rates ($\dot{N}_m$). Time histories in an example hybrid discharge are shown in figure 6(a), where both the classical ($\dot{N}_c$) and the TRANSP-'Kick' model ($\dot{N}_k$) match $\dot{N}_m$ before NTM onset. After NTM onset $\dot{N}_m$ drops as the plasma confinement drops due to the NTM driven transport. Since thermal profiles from the experiment are given as input to TRANSP, the observed deficit ($\Delta\dot{N}_m = \dot{N}_c - \dot{N}_m$) after NTM onset indicates that the FI confinement decreases as well. This effect is quantitatively captured by the 'Kick'-model. In this case, the neutron deficit is about maximum 20% (figure 6(b)) when the NTM magnetic amplitude is about 10 G, and $W \approx 10$ cm.

The level of transport varies by scenario and W with $\Delta\dot{N}_m$ up to 20%. Figure 6(c) shows the 'Kick' neutron deficit ($\Delta\dot{N}_k = \dot{N}_k - \dot{N}_c$) versus $\Delta\dot{N}_m$ in a set of discharges. Here, $\Delta\dot{N}_k$ and $\Delta\dot{N}_m$ were calculated from $\Delta t = \tau_c \approx 100$ ms independent time windows and error bars represent the standard deviation within each window (τ_c is the energy confinement time). The dashed line represents the ideal $\Delta\dot{N}_k = \Delta\dot{N}_m$ condition. The closer the points to this line the better the 'Kick'-model predictions. The model can capture $\Delta\dot{N}_m$ with a few % difference and a consistent overestimation by 3%. From shot to shot, the center of mass of the points follows the measured trend. The islands have 4–11 cm saturated width and have various m/n helicities, including $2/1$, $3/2$, $4/1$ and $7/2$. As

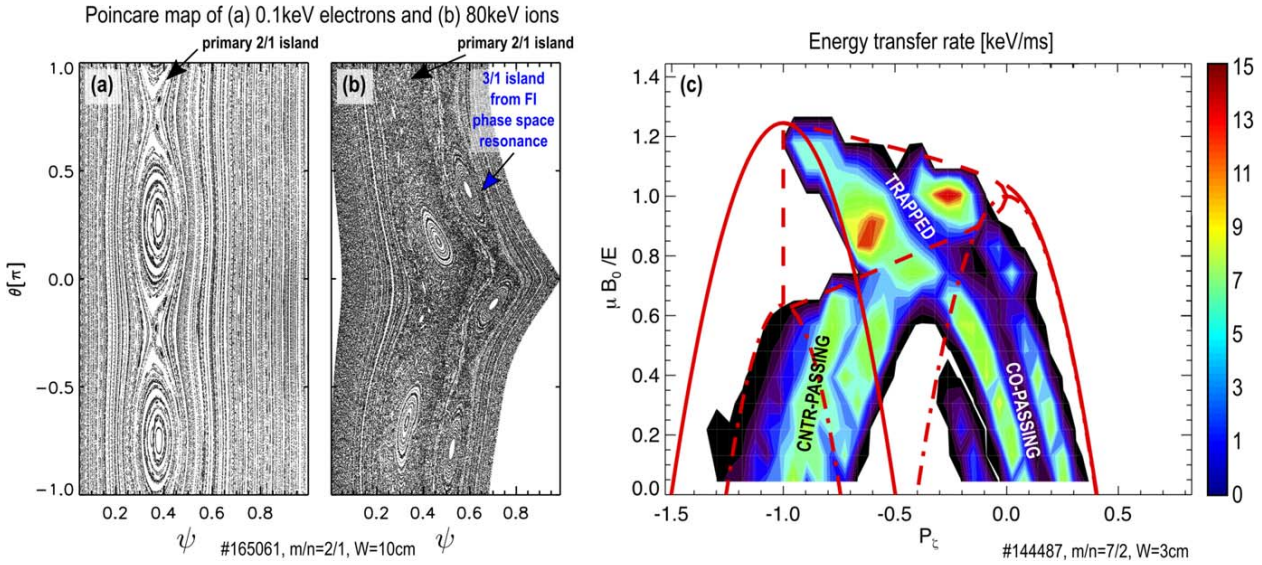

Figure 4. Field line mapping with (a) 0.1 keV electrons and (b) 80 keV co-passing fast ions with $\mu B_o/E = 0.2$. (c) $\dot{E}$ between 55.8 keV FIs and the NTM. For each plot a DIII-D hybrid H-mode plasma equilibrium was used with a $W = 10$ cm, $m/n = 2/1$ magnetic island centered at $\psi_s \approx 0.37$ and rotating with 5 kHz (#165061, see section 2).

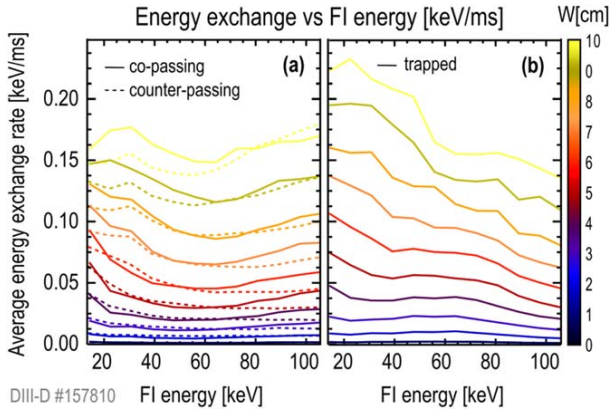

Figure 5. $\dot{E}$ averaged over the (a) co- and counter-passing and (b) trapped particle domains.

mentioned before, W, r_s, m, n and f are all derived from experimental data, therefore the 'Kick'-model has no free parameters.

Note that the preferentially horizontal spread of the points indicates that there is a variation in $\Delta\dot{N}_m$ which is not fully captured by $\Delta\dot{N}_k$. $\Delta\dot{N}_m$ can vary due to (i) the NTM, (ii) other small amplitude modes causing FI transport and (iii) due to the fact that $\dot{N}_c$ does not fully capture the actual classical neutron rates (e.g. fitted profiles are not fully capturing the actual profiles of the discharge). In contrast, $\Delta\dot{N}_k$ only varies due to the NTM (i) as neither TRANSP runs capture other MHD modes and both use the same input profiles.

Next, the scaling of FI transport versus W and f is studied. For this purpose, we use an IBS discharge (DIII-D #157810) with a single $m/n = 3/2$ magnetic island. In section 4.1, W is varied in the experimentally relevant 1–10 cm range in a series of TRANSP analyses, while $f = 22$ kHz is fixed. In section 4.2, f is varied in the 5–50 kHz range at fixed $W = 10$ cm. Results are averaged over the stationary state of each simulation ($\Delta t = 900$ ms). Error bars represent statistical uncertainties of the time averages and were estimated as $\bar{\sigma} = \sigma/\sqrt{N_c - 1}$, where σ is the standard deviation and $N_c = \Delta t/\tau_c$ is the number of independent time windows within the stationary state.

4.1. Scaling of FI transport versus island width

The widths of the real space island structures in the FI population (which are usually not equal to the magnetic island width W), or alternatively the width of phase space resonances, increase with the NTM amplitude ($\widetilde{B}$). Below a critical $\widetilde{B}$, each resonant deterministic FI orbit moves around its own resonance, mapping out a series of non-overlapping island chains (figure 7(a)) at various rational surfaces. These include the $q = 1$ surface near the magnetic axis and several $q > 3/2$ surfaces in the $\psi > 0.55$ region, where equation (3) is satisfied. When $\widetilde{B}$ exceeds a critical value ($\widetilde{B}_c$), the adjacent phase space resonances start to overlap and the FI orbits will move between two or more islands in an unpredictable manner, turning the region of closely spaced island chains into a chaotic region [16, 33, 34] (figure 7(b)). This condition can be expressed in terms of a threshold island width W_{th} where $\widetilde{B}_c \propto W_{th}^2$.

FI losses increase due to the NTM only when $W > W_{th}$ (figure 7(c)). This is in accord with the fact that non-overlapping islands do not alter the FI orbits enough to scatter FIs outside or close to the plasma boundary. When $W > W_{th}$, FI losses grow rapidly with W and reach 270% at $W = 10$ cm (relative to w/o NTM).

A small neutron deficit $\Delta\dot{N}_k$ is observed when $W < W_{th}$ (figure 7(d)), attributed to a small radial redistribution of FIs. This redistribution is evident from the radial profile of p_{FI} (figure 7(g)) as well as from $p_{FI}(W)$ integrated over the whole plasma volume (figure 7(h)). Above the threshold FI losses

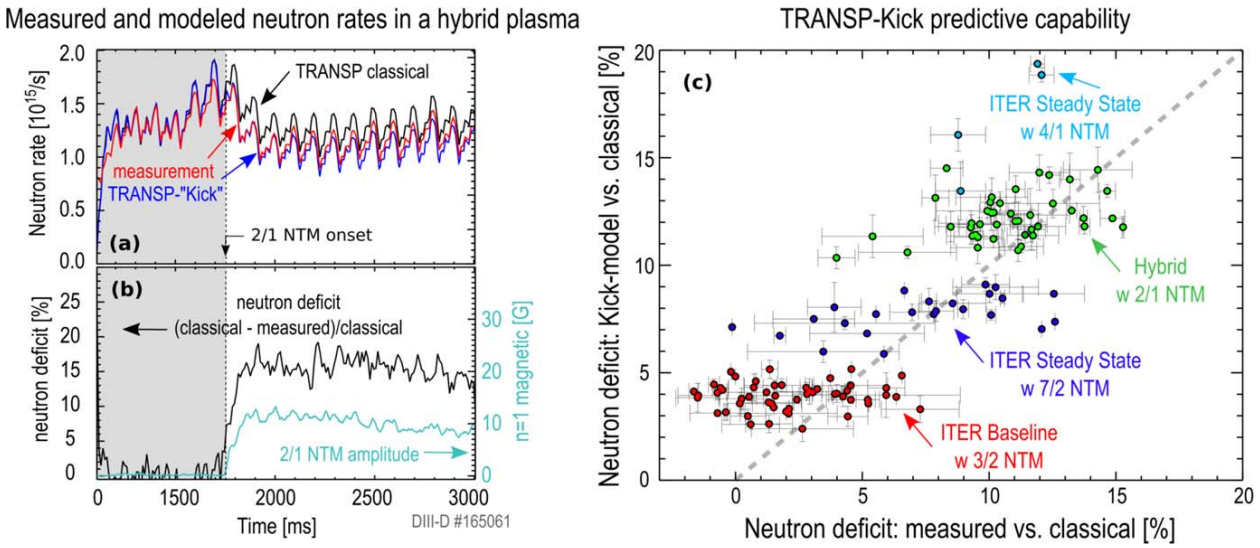

Figure 6. (a) Example of measured and TRANSP neutron rates w and w/o 'Kick' -matrix, (b) neutron deficit and NTM amplitude in a hybrid discharge. (c) 'Kick' versus measured neutron deficit in a set of discharges. Data was calculated from 100 ms independent time windows, error bars represent the standard deviation within each window.

significantly decrease p_{FI} in the $\psi = 0.1$–0.7 radial range and $\Delta\dot{N}_{\mathrm{k}}$ continues to grow as W is further increased.

Similarly to the integral of p_{FI}, there is no change in the integrals of T_{NB} and j_{NB} as long as $W < W_{\mathrm{th}}$ (figures 7(j) and (l), respectively). Resulting from the redistribution, T_{NB} hollows and j_{NB} flattens at $q = m/n$ while both increase near the magnetic axis (figures 7(i) and (k), respectively). When $W > W_{\mathrm{th}}$, the integrals of T_{NB} and j_{NB} decrease, which can be attributed to the FI losses in this regime.

As FI losses leave fewer FIs in the plasma to interact with the NTM at $W > W_{\mathrm{th}}$, the slope of $\dot{E}$ versus W decreases at W_{th}. The resulting break point in $\dot{E}(W)$ allows one to accurately determine W_{th} (figure 7(e)). In this plasma $W_{\mathrm{th}} \approx 4.5$ cm and $\dot{E}$ scales as:

- $\dot{E} \propto W^4 \propto \widetilde{B}^2$ when $W < W_{\mathrm{th}}$ (isolated islands);
- $\dot{E} \propto W^2 \propto \widetilde{B}$ when $W > W_{\mathrm{th}}$ (overlapping islands).

In comparison, the threshold for a locked NTM [6] is about 7.5 cm, which is expected to shift down with rotation as the resonances become stronger when the mode frequency is increased.

NTMs slow down FIs in the $\psi > \psi_s$ region and accelerate them in the $\psi < \psi_s$ region, as seen from the radial profile of $\dot{E}$ (figure 7(f)).

Notice that δj_{NB}, δT_{NB} and $\dot{E}$ have similar radial profiles in the vicinity of ψ_s: these quantities are negative (positive) at $\psi > \psi_s$ ($\psi < \psi_s$) when $W < W_{\mathrm{th}}$ and about zero far from $\psi = \psi_s$. Since $\delta p_{\mathrm{FI}} \approx 0$ when $W < W_{\mathrm{th}}$, $\dot{E}$ offers a qualitative explanation of the radial redistribution of j_{NB} and T_{NB}.

Figure 8 shows δj_{NB} and $\dot{E}$ separately for co-passing, counter-passing and trapped FIs with an island of $W = 7$ cm. $\dot{E}$ is strongest with the trapped FIs. The dip in j_{NB} around $\psi = 0.6$ results from the slow down of co-passing, trapped and counter-passing ions, with the main contribution being attributed to trapped ions. The peak in j_{NB} around $\psi = 0.3$ is dominantly due to the heating of co-passing FIs with some contribution from trapped FIs.

In the IBS discharge (#157810) used here $W \approx 3$ cm and FIs drive the mode with 15 kW (figure 7(d)). In comparison, in a DIII-D experiment [35] (#159243) with many overlapping small amplitude AEs in the $\psi < 0.55$ range (figure 7(a) dashed), $\dot{E}$ between AEs and the FI population is about 28 kW. This, in terms of net $\dot{E}$, corresponds to a 3/2 NTM of $W \approx 3.2$ cm rotating with $f \approx 22$ kHz. Note that FIs have a destabilizing effect on the NTM but stabilizing effect on the AEs in the shown example. It is worth noting that $W \approx 10$ cm islands are not uncommon in this type of plasma, in which case FIs can pump as much power into the NTM as 400 kW. Such NTMs decrease p_{FI}, j_{NB} and T_{NB} by 20%–30% in these integrated TRANSP simulations. This raises several interesting questions and will be the subject of future investigation.

Further tests comparing different NTM representations (appendices A, B) indicate that $\dot{E}$ and the FI losses are nearly the same regardless of the exact shape of Ψ. This indicates that the resonances in the $\psi > \psi_s$ region depend mainly on the maximum of ψ (at ψ_s, which is identical in the two representations) and not on the local values in the edge region. This can be understood as the particle orbits are not localized on rational surfaces but sample a relatively wide radial range including the island region.

4.2. Scaling of FI transport versus mode frequency

Similarly to the amplitude scan reported in section 4.1, in figure 9, a single $m/n = 3/2$ magnetic island is implemented at $q = m/n$. Here the rotation frequency was varied between $f = 2$–50 kHz in a series of TRANSP simulations while $W = 10$ cm was fixed. Recall that wave-particle phase space resonances depend on mode frequency as prescribed by equation (3). The $\psi \gtrsim 0.55$ region is chaotic at all f, however

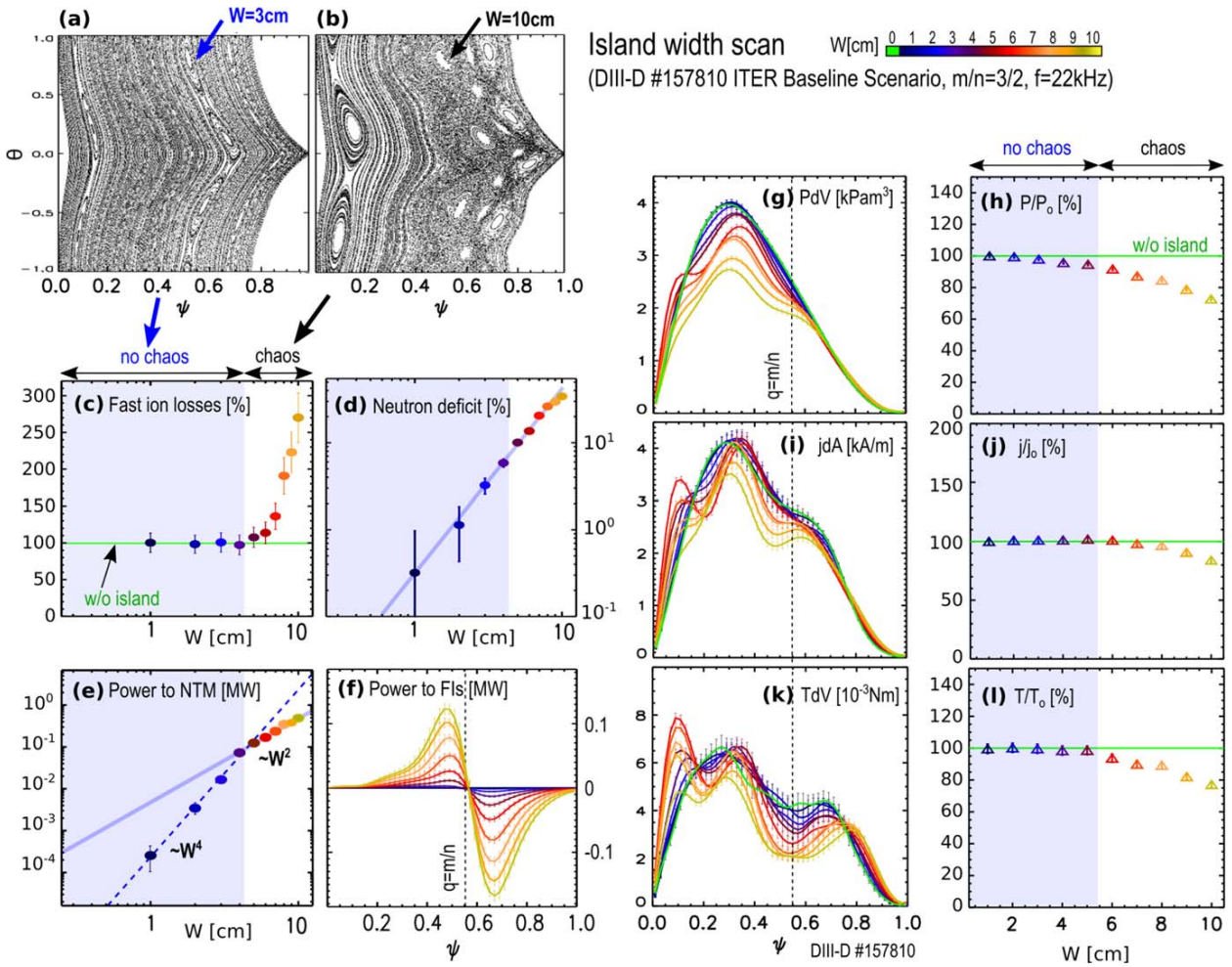

Figure 7. Poincaré maps of 80 keV FIs ($\mu B_o/E = 0.2$) with (a) $W = 3$ cm, (b) $W = 10$ cm. Scaling of (c) FI losses and (d) neutron deficit, (e) $\dot{E}$ versus W. Radial profiles of (f) $\dot{E}$ to FIs, (g) FI pressure, (i) NB current and (k) NB torque (to ions) at different W. Scaling of (h) FI pressure, (j) NB driven current and (l) torque (to ions) integrals over $\psi = [0, 1]$ versus W.

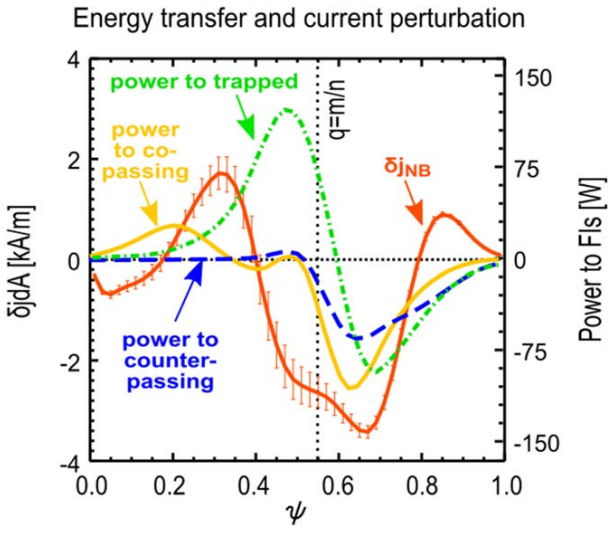

Figure 8. Perturbation of NB current and $\dot{E}$ to different classes of fast ions.

at $\psi \approx 0.3$ an $m = 3$ resonance forms an island in the FI phase space only when $f > f_{cr}$, where $f_{cr} \approx 22$ kHz is the threshold frequency for the core resonance to form. This is shown in the Poincaré plots of 80 keV ions in figures 9(a), (b).

FI losses increase with f when $f < f_{cr}$ (figure 9(c)), which decreases p_{FI} primarily in the $0.2 < \psi < 0.8$ range (figures 9(g), (h)). In turn, $\Delta\dot{N}_k$ rapidly increases with f in this range (figure 9(d)). Note that FI losses and $\Delta\dot{N}_k$ significantly decrease as the mode rotation frequency is lowered. In fact, at $f \gtrsim 0$ kHz, FI losses are reduced to neoclassical levels, i.e. with no island. In this case the island only leads to radial redistribution of FIs near ψ_s. When $f > f_{cr}$ the FI confinement improves inside the $\psi = 0.2$ surface as the mode frequency is increased (figure 9(g)), which leads to a turn over in FI losses and in $\Delta\dot{N}_k$. This effect is solely due to the isolated $m = 3$ resonance in the core at high f, which acts as a transport barrier and improves FI confinement near the magnetic axis.

j_{NB} and T_{NB} qualitatively follow the behavior of p_{FI} (figures 9(i)–(l)). When $f \gtrsim 0$, δj_{NB} and δT_{NB} is negative (positive) at $\psi < \psi_s$ ($\psi > \psi_s$) which leads to hollow (peaked) j_{NB} and T_{NB} profile just inside (outside) the $\psi = \psi_s$ surface.

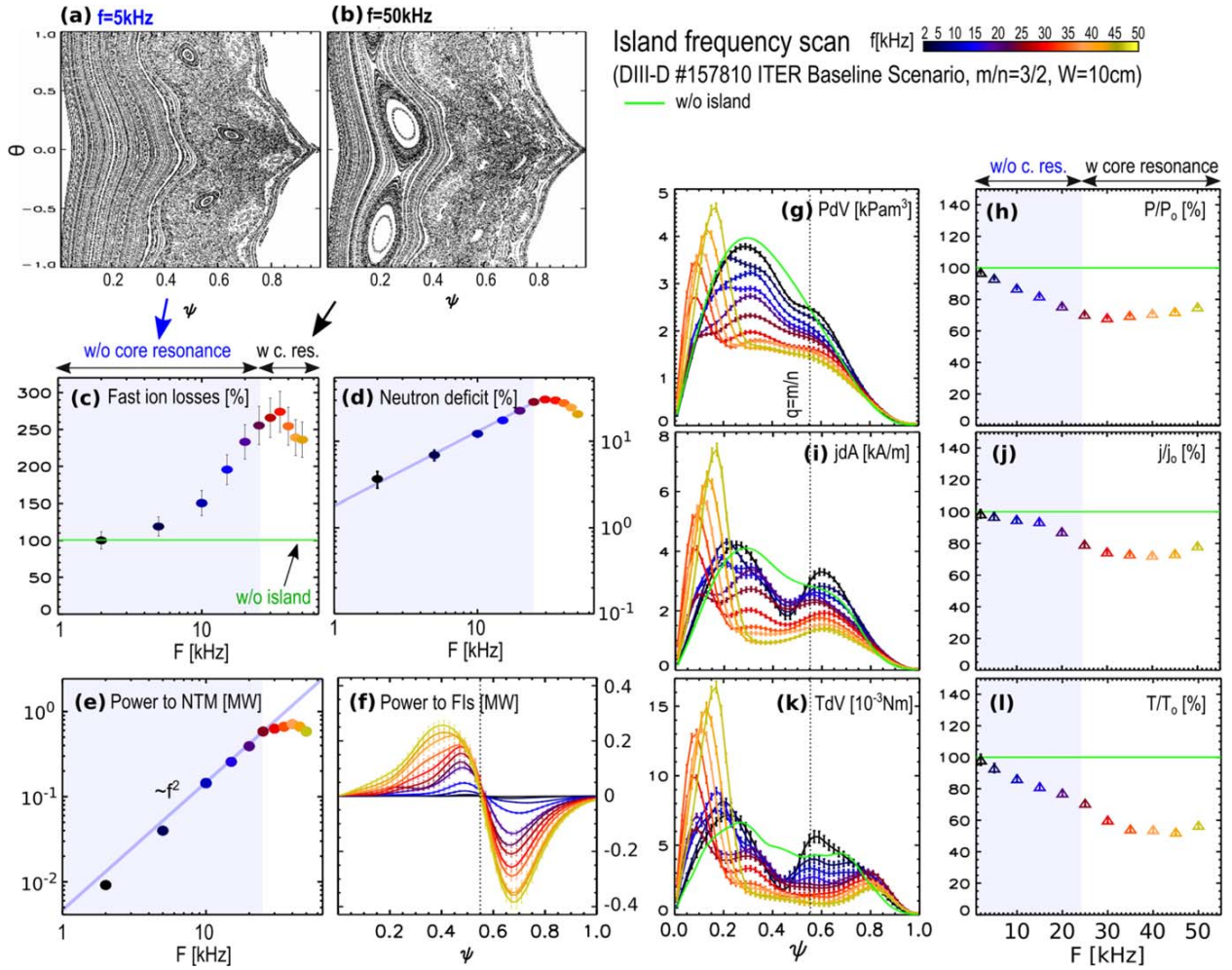

Figure 9. Poincaré maps of 80 keV FIs ($\mu B_o/E = 0.2$) with (a) $f = 5$ kHz, (b) $f = 50$ kHz. Scaling of (c) FI losses and (d) neutron deficit, (e) $\dot{E}$ versus f. Radial profiles of (f) $\dot{E}$ to FIs, (g) FI pressure, (i) NB current and (k) NB torque (to ions) at different f. Scaling of (h) FI pressure, (j) NB current and (l) torque (to ions) integrals over $\psi = [0, 1]$ versus f.

When $0 \gtrsim f < f_{cr}$, the FI losses start to flatten j_{NB} and T_{NB} across ψ_s. When $f > f_{cr}$, j_{NB} and T_{NB} flatten across $0.2 < \psi < 0.8$ and develop a peak inside $\psi \approx 0.2$.

At all frequencies, FIs slow down (accelerate) on the edge (core) side of $q = m/n$ surface (figure 9(f)). Below f_{cr}, $\dot{E} \propto f^2$ (figure 9(e)), which was found valid also for small islands. Recall that $\dot{E} \propto \widetilde{B}^2$ for small islands (section 4.1) and therefore $\dot{E}(W) \propto (\omega\widetilde{B})^2 \propto \widetilde{E}^2$. This indicates that the $\dot{E}$ is due to $\widetilde{E}$ caused by the island rotation and not by the perturbed curvature and $\nabla\widetilde{B}$ drifts. Static islands do not lead to $\dot{E}$ between the FIs and the TM as expected since the work done on charged particles by a static magnetic field is zero.

Recall that in the small island regime with no chaos, δj_{NB} was in accord with $\dot{E}$ (figures 7(f), (i)). In contrast, here j_{NB} increases (decreases) outside (inside) of ψ_s, the opposite way as $\dot{E}$ dictates. This apparent contradiction is resolved by the fact that the particle trajectories are chaotic in the vicinity of $q = m/n$ region at all frequencies when $W = 10$ cm, which locally flattens p_{FI} and moves current radially outward across ψ_s.

Interestingly, $\dot{E}$ also saturates at $f > f_{cr} =$ (figure 9(e)). This occurs due to the broadening of $\dot{E}$ in the $\psi < \psi_s$ region as the $m = 3$ resonance pumps energy into the FI population.

4.3. Comparison to the ad hoc beam ion diffusivity model

Previously, an ad hoc beam diffusivity (χ_{ab}) has been used in TRANSP to account for the effect of NTM driven FI transport on the NB profiles [18, 36]. In the simplest implementation of that model χ_{ab} is spatially uniform and its the magnitude is chosen to match TRANSP $\dot{N}$ to the measurements. χ_{ab} simply broadens the beam profiles without incorporating any of the wave-particle resonant interaction physics in phase space, and has therefore no spatial, E, P_ζ, μ_B or m, n dependence.

Interestingly, despite the lack of real- and phase space sensitivity, several quantities show good agreement with the 'Kick'-model when $\Delta\dot{N}_m$ is matched (figure 10), e.g. the electron thermal diffusivity (χ_e) and FI losses. However, many other important quantities, e.g. the ion thermal diffusivity profile (χ_i), the core FI pressure (p_{FI}), j_{NB} and the

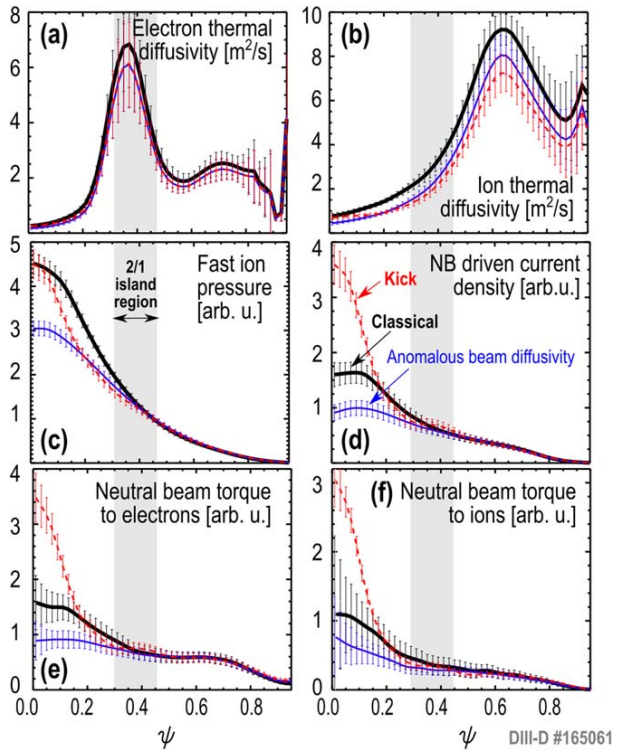

Figure 10. Comparison of the ad hoc diffusivity model and the 'Kick'-model. (a) Electron and (b) ion thermal diffusivity, (c) FI pressure, (d) NB current density, NB torque to (e) electrons and (f) ions.

torque density to the ions and to the electrons can be different. In the shown example with a core $2/1$ island of $W = 10$ cm, which is typical in DIII-D IBS discharges and not uncommon in hybrid plasmas, the differences are large. The χ_{ab} model shows roughly 30% reduction in p_{FI}, j_{NB} and T_{NB} in the core region beyond the NTM rational surface ($\psi < \psi_i = 0.3$). In contrast, the 'Kick'-model shows a maximum reduction in p_{FI} about 15% with no change on the magnetic axis, roughly 100% increase in j_{NB} and T_{NB} to the electrons and 200% increase in T_{NB} to the ions in the $\psi < \psi_i$ region. In the physics-based 'Kick'-model the island redistributes the FI current in the core (figure 10(d)) by redistributing the E and P_ζ around the resonance, decreasing (increasing) j_{NB} and T_{NB} near the resonance (outside the resonance near the plasma magnetic axis). As described in section 4.1, the net effect of the NTM (integrated over the whole plasma volume) is a redistribution when $W < W_{th}$. When $W > W_{th}$, phase space resonance overlaps will lead to FI losses, resulting in an overall decrease of all quantities.

4.4. Impact of mode helicity

Finally, to demonstrate the potential for applications, we have tested the effect of islands with different m/n in a set of simulations using the same plasma equilibrium (figure 11). $2/1$ magnetic islands of $W = 5$ cm lead to a series of overlapping resonances resulting in (i) a chaotic region at $\psi > 0.4$ and (ii) a large $1/1$ island in the FI population at $\psi \approx 0.2$. (i) Reduces j_{NB} in the $0.5 < \psi < 0.8$ region, while (ii) leads to a dip in j_{NB}

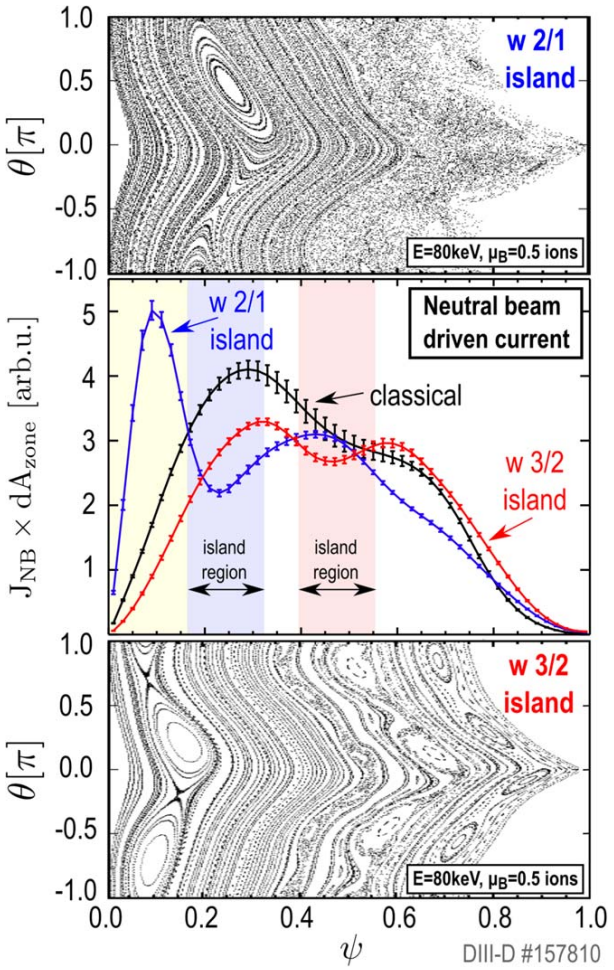

Figure 11. Effect of (a) an $m/n = 2/1$ and (c) an $m/n = 3/2$ NTM on (b) the neutral beam driven current.

at the resonance as well as a peak in j_{NB} near the magnetic axis. For the same plasma equilibrium, a hypothetical $3/2$ NTM of $W = 5$ cm also forms a series of island chains in the $\psi > 0.5$ region. However, in contrast to the $2/1$ NTM, the $3/2$ NTM leads to a resonance n in the $\psi < 0.15$ region which leads to a FI current perturbation δj_{NB} that broadens j_{NB} near the axis. Additionally, this δj_{NB} may form a magnetic island destroying the nested flux surfaces of the equilibrium plasma in a narrow region near the magnetic axis. This change of core topology could result in an additional loss of thermal confinement and current which may be an important mechanism keeping the safety factor above 1 on the magnetic axis of hybrid plasmas. However, this mechanism is only hypothesized here. Further investigation of the problem is not supported in the present version of TRANSP as the toroidal and poloidal symmetry ($m = 0$, $n = 0$) of the profiles are assumed.

5. Summary

We have extended the TRANSP-'Kick' model to include NTM driven FI transport by integrating it with a new analysis

tool of experimental island structure determination. Island evolution is an input and is prescribed entirely through measurements in these interpretive simulations. For predictive simulations, one would have to adopt an NTM dynamic model to advance the island growth and rotation. This model retains all TRANSP functionality and self-consistently recovers the NTM impact on beam torque, current drive and heating. Therefore, this model can be used to design and optimize discharges for tokamak scenario development.

Initial tests with IBS, hybrid and steady state discharges in DIII-D are encouraging as the model quantitatively replicates the measured neutron rate without free parameters.

Two regimes of FI transport have been observed:

- Isolated wave-particle phase space resonances (isolated islands of FIs in real space) lead to a redistribution of the NB driven current and torque without FI losses. These perturbations can be explained by FI–NTM energy transfer without radial redistribution of the FI density. $\dot{E}$ scales with $(\omega\widetilde{B})^2$.
- Overlapping resonances lead to chaotic motion of FIs in a wide radial range between overlapping island chains. Due to the larger $\mathrm{d}q/\mathrm{d}\psi$ in the $\psi > \psi_s$ region, resonance overlaps develop on the edge side of the primary island and lead to FI losses and concomitant loss of NB current and torque, on top of the redistribution. This loss of FIs also reduces the derivative of $\dot{E}$ versus W.

The threshold island width at which resonances start to overlap is at $W \approx 4.5$ cm for the case studied in this paper. In the presented example with a $3/2$ mode the torque profile hollows at the $q = 3/2$ rational surface and the current profile broadens in the core. A frequency scan showed that non-rotating core islands do not lead to the interactions and effects described above. Slowly rotating islands however do lead to FI losses and to perturbations of the FI pressure, NB driven torque and current. The reported effects strongly depend on the particle-wave resonances in phase space which also depend on NTM helicity. In particular, the $m/n = 3/2$ NTM broadens j_{NB} but the $m/n = 2/1$ NTM leads to the peaking of j_{NB} near the magnetic axis. The interaction strength slightly decreases (increases) versus E for co-passing and counter-passing ions at low (high) E. In contrast, trapped ions experience a weaker effect at high E. The strength of the interaction integrated over the whole phase space is nearly independent of $\dot{E}$, which implies that the reported effects are independent of the beam ion injection energy for typical injection energies of present fusion devices.

A more sophisticated FI transport model is under development which will take steps toward self-consistency by integrating the following key elements: (i) linking to the TRANSP NTM module that calculates NTM growth rates [37]; (ii) recalculating the 'Kick'-matrix as the equilibrium changes during the TRANSP simulation; (iii) modify sources as dictated by the FI transport and evolve the equilibrium. The model will also be integrated into the OMFIT [38] workflow to facilitate applications for a wide range of transport analyses of plasmas with NTMs.

Acknowledgments

This research was supported by the General Atomics Post-graduate Research Participation Program administered by ORAU. This material is based upon work supported by the US Department of Energy, Office of Science, Office of Fusion Energy Sciences, using the DIII-D National Fusion Facility, a DOE Office of Science user facility, under Awards DE-FC02-04ER54698, DE-AC02-09CH11466 and DE-AC05-060R23100. DIII-D data shown in this paper can be obtained in digital format by following the links at https://fusion.gat.com/global/D3D_DMP. This report was prepared as an account of work sponsored by an agency of the United States Government. Neither the United States Government nor any agency thereof, nor any of their employees, makes any warranty, express or implied, or assumes any legal liability or responsibility for the accuracy, completeness, or usefulness of any information, apparatus, product, or process disclosed, or represents that its use would not infringe privately owned rights. Reference herein to any specific commercial product, process, or service by trade name, trademark, manufacturer, or otherwise does not necessarily constitute or imply its endorsement, recommendation, or favoring by the United States Government or any agency thereof. The views and opinions of authors expressed herein do not necessarily state or reflect those of the United States Government or any agency thereof.

Appendix A. Representation of tearing modes

NTMs are driven by a three-dimensional helical bootstrap current perturbation (δj) with poloidal and toroidal mode numbers m and n, respectively, and with radial localization at $q = m/n$. $\widetilde{B}$ of δj and the background field (B) organize into a toroidal flux tube around δj, called magnetic island, with nested flux surfaces bounded by a separatrix. These structures are implemented in ORBIT through the $\Psi(r,\ \xi(t),\ t)$ flux, the amplitude of which is chosen to match the experimental island width (W). The non-axisymmetric magnetic field perturbation is $\tilde{\mathbf{B}}(r,\ \xi,\ t) = \nabla \times (\mathbf{e}_z \Psi(r,\ \xi,\ t))$ where $\Psi(r,\ \xi(t),\ t) = \Psi_o(t)\Psi(r)\Psi(\xi(t))$. Here the large tokamak approximation is used and $\mathbf{e}_z$ is the unit vector in the z-direction in cylindrical coordinates. The helical unit vector $\mathbf{e}_\xi$ is perpendicular both to the radial unit vector $\mathbf{e}_r$ and to the equilibrium field line on the $q = m/n$ rational surface. Explicit time dependence of the NTM dynamics are prescribed entirely through $\Psi(t)$ by measurements of the magnetic island width, without a theoretical model being adopted to predict and advance the island growth (see appendices B and C). $\Psi(\xi(t))$ is the helical part, which contains the implicit time dependence in the laboratory frame due to the island rotation and $\Psi(r)$ is the radial part.

The helical part is $\Psi(\xi) = \cos(\xi)$ and the phase is $\xi_i = m\theta_i - n\phi_i$ in the island frame (the index i labels the island frame coordinates). Island rotation in the lab frame evolves the island phase (ξ) as:

$$\xi = \xi_i + \int (m\omega_\theta(t) - n\omega_\phi(t))\mathrm{d}t = \xi_i + \int (\omega(t))\mathrm{d}t. \quad \text{(A1)}$$

Since the phase evolution is prescribed by the $m\omega_\theta(t) - n\omega_\phi(t)$ combination, the measured lab frame frequency $\omega(t)$ can be used to rotate the islands in the numerical implementation.

To derive a model for the radial part $\Psi(r)$ from first principles, we use a model current sheet perturbation localized on a cylindrical surface of radius r_s, flowing parallel to the axis of the cylinder:

$$\tilde{\mathbf{j}}(r, \xi) = \tilde{j}_\circ \cos(\xi)\delta(r_s - r)\mathbf{e}_z = \tilde{j}_\delta(r)\cos(\xi)\mathbf{e}_z. \quad \text{(A2)}$$

Here, r_s is the minor radius coordinate of the $q = m/n$ rational surface and $\tilde{j}_\circ$ is a constant amplitude. Assuming vacuum solutions, the definition of $\tilde{B}$ and Ampère's law yields an equation for the flux $\Psi_\delta(r, \xi)$ of the radially localized current sheet:

$$\nabla^2\Psi_\delta(r, \xi) = \mu_\circ\tilde{j}_\delta(r)\cos(\xi) \quad \text{(A3)}$$

$\mu_\circ$ is the vacuum permittivity. Equation (A3) is solved inside and outside of the $q = 2$ surface analytically. Continuity of the solution across $q = m/n$ is required, while the jump of $\mathrm{d}\Psi/\mathrm{d}r$ is the current flowing at the O-point:

$$\Psi_\delta(r, \xi) = \frac{\mu_\circ\tilde{j}_\circ}{m^2}f(r)\cos(\xi), \quad \text{(A4)}$$

$$f(r) = \frac{r^2}{r_s} \text{ at } r < r_s, \quad f(r) = \frac{r_s^3}{r^2} \text{ at } r > r_s. \quad \text{(A5)}$$

This form was also used in a recent study of locked NTMs [39]. Note that $\partial_r\Psi_\delta$ is discontinuous at r_s due to the assumed δ-like localization of the current sheet. This is averted by solving for a physically more relevant, radially smooth Gaussian current distribution:

$$\mathbf{j}_G(r) = j_G(r)\mathbf{e}_z = j_\circ \exp\left(-\frac{(r - r_s)^2}{2(W/4)^2}\right)\mathbf{e}_z. \quad \text{(A6)}$$

Since expression (A4) is the Green's function of equation (A3), the solution (Ψ_G) with the current defined in (A6) is produced by the convolution of expression (A4) with (A6). To avoid potential numerical problems in ORBIT arising from the discontinuity of $\partial_r\Psi_\delta$, we use Ψ_G in this study, $\Psi(r, \xi) = \Psi_G(r, \xi)$ and $\Psi(r, \xi, t) = \Psi_\circ(t)\Psi_G(r, \xi)$.

Appendix B. Magnetic island structures

The nested flux surfaces of the islands are mapped out by the contours of the total helical flux $\chi(r, \xi)$, the sum of the background and the perturbation flux:

$$\chi(r, \xi) = -\int_r^{r_s}\left(1 - \frac{q}{q_s}\right)B_\theta \mathrm{d}r + \Psi(r, \xi). \quad \text{(B1)}$$

Here, B_θ is the background poloidal magnetic field. Taylor-expanding $\Psi(r)$ and $q(r)$ up to first order about the resonant surface and assuming $B_\theta = $ const. gives:

$$\Omega = 8\frac{(r - r_s)^2}{W^2} + \left(\frac{2A}{W}(r - r_s) + 1\right)\cos(\xi) \quad \text{(B2)}$$

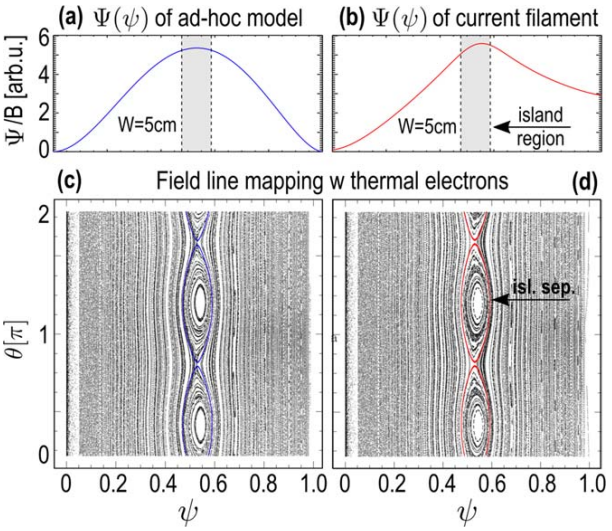

Figure 12. (a), (b) $\Psi(r)$ ($W = 5$ cm, $m/n = 2/1$) and (c), (d) corresponding field line mapping with thermal electrons. Island separatrices are over plotted in (c), (d).

$\chi/\Psi_\circ = \Omega$ is a normalized flux surface label [40] with $\Omega = 1 - A^2/8$ on the island separatrix. W and A are the island width and the radial asymmetry [41], respectively:

$$W = 4\sqrt{\Psi_\circ\frac{L_q(r_s)}{B_\theta(r_s)}}, \quad A = \frac{W}{2}\left\langle\frac{\partial\Psi}{\partial r}\right\rangle. \quad \text{(B3)}$$

Here, $L_q(r_s) = q(r_s)/(\partial_r q)_{r_s}$ is the magnetic field shear length scale at r_s. The 'constant-Ψ' approximation [42] ($A = 0$) leads to islands that are symmetric about the resonant surface. Typically $A = -0.6$ in the experiments.

Note that making use of the relationship between $\Psi_\circ$ and W (expression (B3)), $\Psi(r, \xi)$ can be parametrized with W. First, relate $\mu_\circ\tilde{j}_\circ$ to $\Psi_\circ$ via averaging expression (A4) over the island region and assuming $A = 0$:

$$\Psi_\circ \approx \langle\Psi(r)\rangle_{\pm W/2} = \frac{\mu_\circ\tilde{j}_\circ}{4}\bar{f}_W. \quad \text{(B4)}$$

Then using expressions (B3), (B4) the parametrization of $\Psi(r, \xi(t), t)$ with $W(t)$ is:

$$\Psi_\delta(r, \xi(t), t) = \frac{W(t)^2 B_\theta}{16L_q}\frac{f(r)}{\bar{f}_W}\cos(\xi(t)). \quad \text{(B5)}$$

As W, L_q and B_θ can be obtained from experiments rigorously, the 'Kick' NTM–FI transport model can be constructed without any free parameters.

When representing MHD modes in the ORBIT code [43], the $\mathbf{e}_z\Psi(r, \xi) = \mathbf{B}(r)\alpha(r, \xi)$ notation is used. Historically an ad hoc form (α_{AH}) has been adopted in numerical studies [9, 16]:

$$\alpha_{\mathrm{AH}}(r) = \alpha_\circ\left(\frac{r(\psi)}{x_\circ}\right)^m\left(\frac{1 - r}{1 - x_\circ}\right)^{m(x_\circ^{-1} - 1)}. \quad \text{(B6)}$$

Radial profiles of these two representations (Ψ and $\Psi_{\mathrm{AH}} = \mathbf{B}(r)\mathbf{e}_z\alpha_{\mathrm{AH}}(r, \xi)$) are shown in figures 12(a), (b) along with field line tracing in figures 12(c), (d), respectively. Note

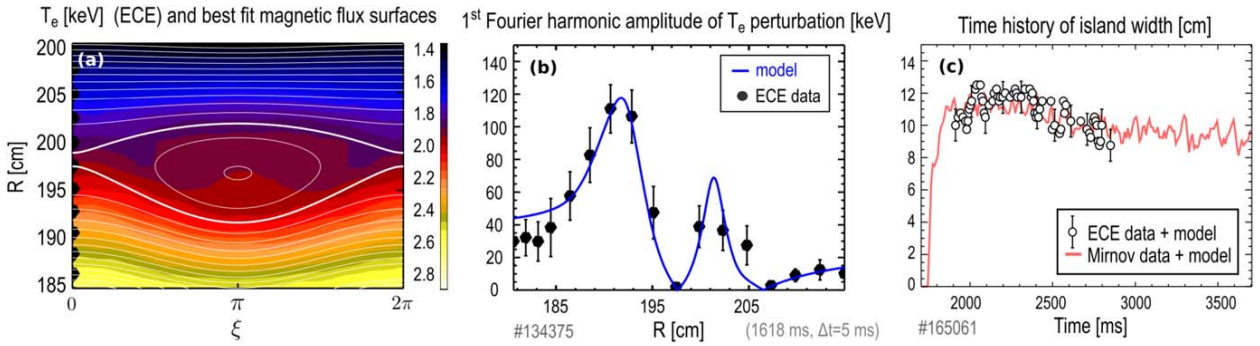

Figure 13. (a) Phase lock averaged T_e (filled contours) and the flux surfaces of a magnetic island that produces the best matched model to the T_e data. The thick solid line is the $\Omega = 1$ flux surface of the island. (b) First Fourier harmonic amplitude of measured and model T_e perturbation. (c) Time history of island width derived from combined ECE and Mirnov data and modeling. Figures (a) and (b) reprinted from [22], with the permission of AIP Publishing.

that (i) the island structures appear to be very similar but (ii) $\Psi_{AH}(\psi = 1) = 0$ while $\Psi(\psi = 1) \approx \max\{\Psi\}/2$. Parameters to constrain experimentally are the island frequency ($f = \omega/(2\pi)$), mode numbers (m and n), radial location of the mode rational surface (ψ_s), the island radial asymmetry (A) and the island width (W).

Appendix C. Determination of island parameters in the experiments

Ω is obtained from Fourier-analysis of ECE data, m and n are determined from poloidal and toroidal Mirnov-coil array data via the Newspec code [29]. The best estimator of $W(t)$, $A(t)$ and $r_s(t)$ are determined in the experiment simultaneously in a series of 5 ms windows by fitting the solutions of an anisotropic heat transport model of magnetic islands to the phase lock averaged electron temperature (T_e) data (figures 13(a), (b)) via least squares method [22]. This gives $W(t)$ when the islands are large and when T_e is available. $W(t)$ is then extended by mapping the magnetic data as

$$W(t) = \alpha B_\theta^2 L_q \left(\frac{r_m}{r_s}\right)^{m+1}. \qquad \text{(C1)}$$

(Figure 13(c)) assuming that the island center is well aligned with the $q = m/n$ rational surface. Here, α is a geometric fit parameter, B_θ and L_q are the equilibrium poloidal magnetic field and magnetic field shear length at r_s, respectively. r_s (r_m) is the mode rational surface (Mirnov-probe) minor radius coordinate. NTM evolution is prescribed entirely by these measurements without a theoretical model being adopted to predict and advance the island growth.

The typical ranges of experimental values are $\omega =$ 5–20 kHz, $m/n = 2/1$, $3/2$, $4/1$ and $7/2$, $\psi_s = 0.4$–0.6, $-0.8 < A < -0.4$ and $W = 3$–10 cm in the saturated state.

ORCID iDs

L Bardóczi https://orcid.org/0000-0002-8280-2423
M Podestà https://orcid.org/0000-0003-4975-0585
W W Heidbrink https://orcid.org/0000-0002-6942-8043
M A Van Zeeland https://orcid.org/0000-0002-7911-2739

References

[1] Gunter S, Gude A, Maraschek M, Yu Q and The ASDEX Upgrade Team 1999 Influence of neoclassical tearing modes on energy confinement *Plasma Phys. Control. Fusion* **41** 767–74
[2] Buttery R J *et al* 2000 Neoclassical tearing modes *Plasma Phys. Control. Fusion* **42** B61–73
[3] Bardóczi L, Rhodes T L, Bañón Navarro A, Sung C, Carter T A, La Haye R J, Petty C, Crystal C and Jenko F 2017 Impact of neoclassical tearing mode—turbulence multi-scale interaction in confinement degradation and magnetic island stability *Phys. Plasmas* **24** 122503
[4] Chang Z and Callen J D 1990 Global energy confinement degradation due to macroscopic phenomena in tokamaks *Nucl. Fusion* **30** 219
[5] Mynick H E and Krommes J A 1979 Particle diffusion by magnetic perturbations of axisymmetric geometries *Phys. Rev. Lett.* **43** 1506
[6] Mynick H E 1993 Transport of energetic ions by low-n magnetic perturbations *Phys. Fluids* B **5** 1471
[7] Konovalov S V and Putvinskii S V 1988 Effect of kink perturbations of the magnetic field on the fast-particle drift surfaces in a tokamak *Sov. J. Plasma Phys.* **5** 1471
[8] Forest C B, Ferron J R, Gianakon T, Harvey R W, Heidbrink W W, Hyatt A W, La Haye R J, Murakami M, Politzer P A and John H E St. 1997 Reduction in neutral beam driven current in a tokamak by tearing modes *Phys. Rev. Lett.* **79** 427
[9] Gobbing M, Marelli L, Fahrbach H U, García-Muñoz M, Günter S, Martin P, White R B and The ASDEX Upgrade Team 2009 Numerical simulations of fast ion loss measurements induced by magnetic islands in the asdex upgrade tokamak *Nucl. Fusion* **49** 095021
[10] García-Muñoz M, Martin P, Fahrbach H-U, Gobbin M, Unter S G, Maraschek M, Marelli L, Zohm H and The ASDEX Upgrade Team 2007 Ntm induced fast ion losses in asdex upgrade *Nucl. Fusion* **47** L10–7
[11] Poli E, García-Muñoz M, Fahrbach H-U, Günter S and ASDEX Upgrade Team 2008 Observation and modeling of fast trapped ion losses due to neoclassical tearing modes *Phys. Plasmas* **15** 032501

[12] Zweben S J, Boivin R L, Diesso M, Hayes S, Hendel H W, Park H and Strachan J D 1990 Loss of alpha-like mev fusion products from tftr *Nucl. Fusion* **30** 1551–74
[13] Zweben S J, Darrow D S, Fredrickson E D, Taylor G, von Goeler S and White R B 1999 Mhd induced alpha particle loss in tftr *Nucl. Fusion* **39** 1097
[14] Zhang Y P *et al* The HL-2A Team 2015 Measurements of fast-ion losses induced by mhd instabilities using a scintillator-based probe in the HL-2A tokamak *Nucl. Fusion* **55** 113024
[15] Pritchard D C, Gandy R F, Hanson J D, Knowlton S F, Lin H, Sasser G E, Thomas E Jr. and Cooney J 1997 Effects of applied rotating magnetic perturbations on ion drift orbits in the compact auburn torsatron *Phys. Plasmas* **4** 162
[16] Carolipio E M, Heidbrink W W, Forest C B and White R B 2002 Simulations of beam ion transport during tearing modes in the diii-d tokamak *Nucl. Fusion* **42** 853
[17] Sauter O *et al* 1997 Beta limits in long-pulse tokamak discharges *Phys. Plasmas* **4** 1654
[18] Hawryluk R J 1981 An empirical approach to tokamak transport *Physics of Plasmas Close to Thermonuclear Conditions* vol 1 (Oxford: Pergamon) 19–46
[19] Poli F, Sachdev J, Breslau J, Gorelenkova M and Yuan X 2018 TRANSP. [Computer software]
[20] Podestà M, Gorelenkova M, Gorelenkov N N and White R B 2017 Computation of Alfvén eigenmode stability and saturation through a reduced fast ion transport model in the transp tokamak transport code *Plasma Phys. Control. Fusion* **59** 095008
[21] Podestà M, Gorelenkova M and White R B 2014 A reduced fast ion transport model for the tokamak transport code transp *Plasma Phys. Control. Fusion* **56** 055003
[22] Bardóczi L, Rhodes T L, Carter T A, Crocker N A, Peebles W A and Grierson B A 2016 Non-perturbative measurement of cross-field thermal diffusivity reduction at the o-point of $2/1$ neoclassical tearing mode islands in the diii-d tokamak *Phys. Plasmas* **23** 052507
[23] Poli F M, Fredrickson E D, Henderson M A, Kim S-H, Bertelli N, Poli E, Farina D and Figini L 2018 Electron cyclotron power management for control of neoclassical tearing modes in the iter baseline scenario *Nucl. Fusion* **58** 016007
[24] Pankin A, McCune D, Andre R, Bateman G and Kritz A 2004 The tokamak monte carlo fast ion module nubeam in the national transport code collaboration library *Comput. Phys. Commun.* **159** 157–84
[25] Heidbrink W W *et al* 2018 The phase-space dependence of fast-ion interaction with tearing modes *Nucl. Fusion* **58** 082027
[26] Van Zeeland M A, Boivin R L, Carlstrom T N, Deterly T and Finkenthal D K 2006 Fiber optic two-color vibration compensated interferometer for plasma density measurements *Rev. Sci. Instrum.* **77** 10F325
[27] Austin M E and Lohr J 2003 Electron cyclotron emission radiometer upgrade on the diii-d tokamak *Rev. Sci. Instrum.* **74** 1457
[28] Burrell K H, Gohil P, Groebner R J, Kaplan D H, Robinson J I and Solomon W M 2004 Improved charge-coupled device detectors for high-speed, charge exchange spectroscopy studies on the diii-d tokamak *Rev. Sci. Instrum.* **75** 3455
[29] Strait E J 2006 Magnetic diagnostic system of the diii-d tokamak *Rev. Sci. Instrum.* **77** 023502
[30] White R B and Chance M S 1984 Hamiltonian guiding center drift orbit calculation for plasmas of arbitrary cross section *Phys. Fluids* **27** 2455
[31] Lao L L, Ferron J R, Groebner R J, Howl W, John H St, Strait E J and Taylor T S 1990 Equilibrium analysis of current profiles in tokamaks *Nucl. Fusion* **30** 1035
[32] Wróblewski D and Lao L L 1992 Polarimetry of motional stark effect and determination of current profiles in diii-d (invited) *Rev. Sci. Instrum.* **63** 5140
[33] White R B 2012 Modification of particle distributions by mhd instabilities i *Commun. Nonlinear Sci. Numer. Simul.* **17** 2200–14
[34] Chirikov B V 1960 Resonance processes in magnetic traps *J. Nucl. Energy* C **1** 253
[35] Collins C S, Heidbrink W W, Podestà M, White R B, Kramer G J, Pace D C, Petty C C, Stagner L, Van Zeeland M A, Zhu Y B and The DIII-D Team 2017 Phase-space dependent critical gradient behavior of fast-ion transport due to Alfvén eigenmodes *Nucl. Fusion* **57** 086005
[36] Pace D C *et al* 2018 Dynamic neutral beam current and voltage control to improve beam efficacy in tokamaks *Phys. Plasmas* **25** 056109
[37] Poli F M 2018 Integrated tokamak modeling: when physics informs engineering and research planning *Phys. Plasmas* **25** 055602
[38] Meneghini O *et al* 2015 Integrated modeling applications for tokamak experiments with omfit *Nucl. Fusion* **55** 083008
[39] Sweeney R, Choi W, La Haye R J, Mao S, Olofsson K E J, Volpe F A and The DIII-D Team 2016 Statistical analysis of $m/n = 2/1$ locked and quasi-stationary modes with rotating precursors at diii-d *Nucl. Fusion* **57** 016019
[40] Fitzpatrick R 1995 Helical temperature perturbations associated with tearing modes in tokamak plasmas *Phys. Plasmas* **2** 825
[41] De Lazarri D and Westerhof E 2011 The role of asymmetries in the growth and suppression of neoclassical tearing modes *Plasma Phys. Control. Fusion* **53** 035020
[42] Furth H P, Killeen J and Rosenbluth M N 1963 Finite-resistivity instabilities of a sheet pinch *Phys. Fluids* **6** 459
[43] White R B 2013 Representation of ideal magnetohydrodynamic modes *Phys. Plasmas* **20** 022105